

Quasi-normal modes of rotating relativistic stars - neutral modes for realistic equations of state

Sharon M. Morsink¹, Nikolaos Stergioulas², and Steve R. Blattnig¹

ABSTRACT

We compute zero-frequency (neutral) quasi-normal f -modes of fully relativistic and rapidly rotating neutron stars, using several realistic equations of state (EOSs) for neutron star matter. The zero-frequency modes signal the onset of the gravitational radiation-driven instability. We find that the $l = m = 2$ (bar) f -mode is unstable for stars with gravitational mass as low as $1.0 - 1.2M_{\odot}$, depending on the EOS. For $1.4M_{\odot}$ neutron stars, the bar mode becomes unstable at $83\% - 93\%$ of the maximum allowed rotation rate. For a wide range of EOSs, the bar mode becomes unstable at a ratio of rotational to gravitational energies $T/W \sim 0.07 - 0.09$ for $1.4M_{\odot}$ stars and $T/W \sim 0.06$ for maximum mass stars. This is to be contrasted with the Newtonian value of $T/W \sim 0.14$. We construct the following empirical formula for the critical value of T/W for the bar mode, $(T/W)_2 = 0.115 - 0.048 M/M_{\max}^{\text{sph}}$, which is insensitive to the EOS to within $4 - 6\%$. This formula yields an estimate for the neutral mode sequence of the bar mode as a function only of the star's mass, M , given the maximum allowed mass, M_{\max}^{sph} , of a nonrotating neutron star. The recent discovery of the fast millisecond pulsar in the supernova remnant N157B, supports the suggestion that a fraction of proto-neutron stars are born in a supernova collapse with very large initial angular momentum. If some neutron stars are born in an accretion-induced-collapse of a white dwarf, then they will also have very large angular momentum at birth. Thus, in a fraction of newly born neutron stars the instability is a promising source of continuous gravitational waves. It could also play a major role in the rotational evolution (through the emission of angular momentum) of merged binary neutron stars, if their post-merger angular momentum exceeds the maximum allowed to form a Kerr black hole.

Subject headings: instabilities — relativity — stars: neutron — stars: oscillations — stars: rotation

¹Department of Physics, University of Wisconsin-Milwaukee,
PO Box 413, Milwaukee, WI 53201, USA
morsink@pauli.phys.uwm.edu; srb2@csd.uwm.edu

²Max Planck Institute for Gravitational Physics (Albert-Einstein-Institute)
D-14473 Potsdam, Germany
niksterg@aei-potsdam.mpg.de

1. Introduction

A core-collapse supernova or the accretion-induced-collapse of a white dwarf can result in the birth of a hot, rapidly rotating neutron star. During the first year of its life (while it cools from $\sim 10^{10} - 10^9\text{K}$) the neutron star will be unstable to the emission of gravitational radiation due to the Chandrasekhar-Friedman-Schutz (CFS) nonaxisymmetric instability (Chandrasekhar 1970; Friedman & Schutz 1978; Friedman 1978). The instability will only be operating while the star is rotating more rapidly than some critical angular velocity. Via the instability, gravitational waves carry away a significant amount of the star's angular momentum. This early spin-down epoch has two important astrophysical implications: First, the gravitational radiation emitted may be detectable by the planned gravitational wave detectors. (Note that this discussion is also relevant to post-merger objects in a neutron star binary coalescence.) Second, it may be possible to indirectly observe the critical angular velocity through the detection of young, rapidly rotating pulsars in supernova remnants, such as PSR J0537-6910 (Marshall et al. 1998).

The critical velocity for the onset of the CFS-instability in polar perturbations, (f -modes) has been computed before in various approximations: in the Newtonian limit (Managan 1985; Imamura, Friedman, & Durisen 1985; Ipser & Lindblom 1990), the post-Newtonian approximation (Cutler 1991; Cutler & Lindblom 1992; Lindblom 1995), and the relativistic Cowling approximation for polytropes (Yoshida & Eriguchi 1997) and realistic equations of state (EOSs) (Yoshida & Eriguchi 1998). For a detailed review, see Stergioulas (1998). The first fully-relativistic computation of the onset of the instability in f -modes is presented in Stergioulas (1996) and Stergioulas & Friedman (1998, hereafter SF). SF find a gauge in which six perturbed field equations can be solved simultaneously on a finite grid with good accuracy. Using polytropic equations of state with index $N = 1.0, 1.5$ and 2.0 , SF show that general relativity has a significant effect on the onset of the instability, lowering the rotation rate at which it occurs, as the star becomes more relativistic. A surprising result is that the $l = m = 2$, “bar” f -mode instability (which in the Newtonian limit exists only for stiff polytropes of index $N < 0.808$) exists for relativistic polytropes with index as large as $N = 1.3$. SF suggested that the $l = m = 2$ instability should also exist for realistic EOSs, which is confirmed in the present paper. In the Newtonian limit the gravitational-wave-driven

and viscosity-driven bar mode instabilities occur at the same value of the ratio of rotational energy to the gravitational binding energy, $T/W \sim 0.14$. SF conjectured that when effects due to relativity are included, the onset of the two types of instabilities will be split, with the CFS instability occurring at lower values of T/W and the viscosity-driven instability at higher values. Calculations of relativistic effects on the viscous instability (Shapiro & Zane 1997; Bonazzola, Friebe, & Gourgoulhon 1998) agree with this conjecture.

For a perturbation with azimuthal angular dependence $e^{im\phi}$, modes with the smallest value of the spherical harmonic multipole index l will have the fastest growth rate and the highest gravitational radiation luminosity. Hence the modes with $l = m$ and in particular, with $m = 2$, are the most relevant for astrophysics. For a perfect fluid all modes with $m \geq 2$ are of interest, however, when imperfect fluid effects are included, (Cutler and Lindblom 1987; Ipser and Lindblom 1991; Lindblom 1995; Yoshida & Eriguchi 1995) polar modes with $m > 5$ will always be damped by shear and bulk viscosity.

In the present paper, we use the SF scheme to determine the onset of the CFS instability of f -modes with $l = m$ and $2 \leq m \leq 5$ for realistic EOSs. We also improve on the numerical implementation of the method, by using a new finite-difference scheme in the angular direction and an improved algorithm for locating the exact onset of the instability with higher accuracy. We find that the realistic EOSs show similar behaviour as the polytropic EOSs in SF. The $l = m = 2$ f -mode becomes unstable for all realistic EOSs examined, for stars with masses as low as $M = 1.0 - 1.2M_{\odot}$, depending on the EOS. Stars with mass near $1.4M_{\odot}$ are unstable to the bar mode at 83% – 93% of the mass-shedding (Kepler) limit.

As was first noticed by Andersson (1998), the critical angular velocity for axial r -modes, in a perfect fluid star, is exactly zero, so that all stars are generically unstable for all values of m (Friedman & Morsink 1998). Again, the inclusion of viscosity will stabilize all modes except those with the lowest values of m . Two independent computations including the effects of viscosity in Newtonian stars (Lindblom, Owen & Morsink 1998; Andersson, Kokkotas & Schutz 1998) estimate that the lowest angular velocity for which $l = m = 2$ r -mode is unstable is roughly 6% – 20% of the Kepler limit for uniformly rotating stars.

The following scenario may describe the early spin-

evolution of a newly born neutron star, if it is born with an angular velocity close to the Kepler limit Ω_K . While the star cools from $\sim 10^{10}\text{K}$ to 10^9K , viscous effects will be small enough that the gravitational radiation instability will spin down the star. In this temperature window the spin evolution will go through two phases. In the first phase, the star is rotating fast enough that both f - and r -modes will be unstable. During the second phase, only the r -modes are unstable. The determination of which mode will be the dominant mechanism for the shedding of angular momentum during the first phase will depend on the relative growth times for both types of modes. At present, the growth times for neither type of mode have been determined for rapidly rotating relativistic stars.

The plan of this paper is as follows. In section 2 we briefly review the method for computing the onset of the polar-mode nonaxisymmetric instability in relativistic stars. In section 3 we present the improvements in the numerical implementation of the scheme. The equations of state selected are discussed in section 4. In section 5 we present the critical angular velocities for f -modes with $2 \leq m \leq 5$ for a variety of equations of state. Astrophysical implications will be discussed in the concluding section.

2. Nonaxisymmetric Perturbations

2.1. Quasi-normal Modes and the Onset of Instability

Taking advantage of the axisymmetry and stationarity of the equilibrium star, a general linear perturbation can be written as a sum of quasi-normal modes, characterized by the spherical harmonic indices (l, m) . In this way perturbations of scalars, such as the energy density can be analyzed as

$$\delta\epsilon = \epsilon_l(r)P_l^m(\cos\theta)e^{i(\omega_i t + m\phi)}, \quad (1)$$

where $P_l^m(\cos\theta)$ are the Legendre functions and ω_i is the frequency of the mode in the inertial frame. Perturbations of vector quantities, such as the four-velocity, can be written in terms of vector harmonics, while the perturbation in the metric can be written in terms of scalar, vector and tensor harmonics (see Regge and Wheeler 1957). Vector and tensor harmonics are of two types - polar, which transform as $(-1)^l$ under a parity transformation (under the combination of reflection in the equatorial plane and rotation by π) and axial, which transform as $(-1)^{l+1}$ under parity. The angular part of polar vector harmonics are

proportional to gradients of the spherical harmonics, while axial vector harmonics are proportional to the curl of a radial vector and a polar vector harmonic.

In the spherical limit, nonaxisymmetric perturbations decouple into purely polar and purely axial modes with unique values of m and l . In a fluid, polar modes correspond to the f -, p - and g - modes in the Newtonian limit, while axial modes correspond to r -modes in a Newtonian star (Papaloizou and Pringle 1978).

In a rotating star, the spherical symmetry is broken. While a mode can still be specified by a single value of m , the mode will no longer consist of a single l harmonic. A polar (l, m) mode acquires higher order, in l , polar terms, due to the non-sphericity of equipotential surfaces, and $(l \pm 1, m)$ and higher order, in l , axial terms, due to the coupling between polar and axial terms:

$$P_l^{rot} \sim \sum_{l'=0}^{\infty} (P_{l+2l'} + A_{l+2l'\pm 1}). \quad (2)$$

Similarly, an axial mode in a rotating star is written as a sum of axial and polar terms:

$$A_l^{rot} \sim \sum_{l'=0}^{\infty} (A_{l+2l'} + P_{l+2l'\pm 1}). \quad (3)$$

Thus, a normal mode of oscillation in a rotating star is defined as polar, if it reduces to a purely polar mode in the nonrotating limit and similarly for axial modes.

Gravitational radiation drives a polar or axial mode of oscillation unstable, whenever the star rotates fast enough, that a perturbation which counter-rotates in the star's rest frame, appears to co-rotate with respect to a distant, inertial, observer. Conservation of angular momentum dictates that the mode's angular momentum must decrease. However, a counter-rotating perturbation's angular momentum (invariantly defined in the rotating frame), is negative, so that gravitational radiation causes a negative angular momentum perturbation to become more negative. For a given value of m , the instability first sets in via an $l = m$ mode, when the frequency of the mode vanishes in the inertial frame. Thus, the problem of finding the critical angular velocity reduces to finding solutions of the time-independent (zero-frequency) perturbation equations.

2.2. Solving for Time-independent Perturbations

In this paper we will follow the method of Stergioulas & Friedman (1998), where one can find a de-

tailed presentation. Here we will only briefly sketch the solution method. In section 3 we will summarize improvements in the numerical implementation.

In writing the perturbation equations for an axisymmetric and stationary, relativistic star, the Eulerian approach is followed (see Ipser & Lindblom 1992 and Friedman & Ipser 1992). The Eulerian perturbations in the metric tensor, $\delta g_{ab} \equiv h_{ab}$, energy density $\delta\epsilon$ and four-velocity δu^a are obtained by solving the system of equations consisting of the perturbed field equations and the perturbed equation of conservation of the stress-energy tensor:

$$\delta R_{ab} = 8\pi\left(\delta T_{ab} - \frac{1}{2}g_{ab}\delta T - \frac{1}{2}h_{ab}T\right), \quad (4)$$

$$\delta(\nabla_a T^{ab} = 0), \quad (5)$$

where a perfect fluid stress-energy tensor

$$T_{ab} = (\epsilon + P)u^a u^b + P g_{ab}, \quad (6)$$

is assumed. In equation (6), ϵ is energy density, P is pressure and u^a is the four-velocity of the fluid.

Since linear perturbations are subject to a gauge freedom, only six components of the perturbed field equations need to be solved. The projection of equation (5) normal to the four-velocity of the fluid i.e. the perturbed Euler equations, can be solved analytically for δu^a . Next, one defines a function

$$\delta U = u_a \delta u^a + \frac{1}{2}u^b u^c h_{bc}, \quad (7)$$

so that the perturbation in the energy density becomes

$$\delta\epsilon = \frac{(\epsilon + P)^2}{P\Gamma}(\delta U + \frac{1}{2}u^a u^b h_{ab}), \quad (8)$$

where

$$\Gamma = \frac{\epsilon + P}{P} \frac{dP}{d\epsilon} \quad (9)$$

is the adiabatic index of the perturbation (assumed to be equal to the adiabatic index of the equilibrium fluid).

Thus, a zero-frequency mode is obtained by solving six components of the perturbed field equations (4) for h_{ab} and the perturbed energy conservation equation

$$\delta(u_b \nabla_a T^{ab} = 0), \quad (10)$$

for δU . SF found that by choosing the gauge as

$$h_{r\theta} = 0, \quad (11)$$

$$h_{\theta\phi} = 0, \quad (12)$$

$$h_{t\phi} = -\omega h_{\phi\phi}, \quad (13)$$

$$h_{\phi\phi} = \frac{h_{\theta\theta}}{r^2} e^{2(\psi-\alpha)}, \quad (14)$$

six components of the perturbed field equations can be solved simultaneously on a finite grid for the required boundary conditions, given a trial function for δU that is close to its actual solution.

The remaining equation (10) is solved by expanding the function δU in terms of suitably chosen basis functions δU_i

$$\delta U = \sum_i a_i \delta U_i. \quad (15)$$

For polar modes, the basis functions are chosen to be

$$\delta U_i = \delta U_i^{(jk)} = r^{l+2(j+k)} Y_{l+2k}^m(\cos\theta), \quad (16)$$

obtained by letting j and k take different values ≥ 0 for each value of i . Equation (10) is an equation linear in δU and can be represented schematically as

$$L(\delta U) = 0, \quad (17)$$

where L is the linear operator defined in Appendix C of SF. Substituting the expansion (15) in equation (17) and defining the inner product

$$\langle \delta U_j | L | \delta U_i \rangle = \int i \frac{\delta U_j}{m\Omega u^t} L(\delta U_i) \sqrt{-g} d^3x, \quad (18)$$

where Ω is the angular velocity of the star, a solution for the homogeneous equation (17) exists, only when the determinant of the inner product matrix vanishes,

$$\det \langle \delta U_j | L | \delta U_i \rangle = 0. \quad (19)$$

The solution to the perturbation equations is found by successively solving the perturbed field equations for a trial function of the form given by equation (15) and then evaluating the determinant of equation (18) for a sequence of stars with increasing rotation rate until the determinant's value passes through zero. The star for which the determinant is exactly zero, has a zero-frequency (neutral) f -mode, indicating the onset of the gravitational-radiation driven instability in this mode.

Stergioulas & Friedman (1998), also found that neutral f -modes can be determined with high accuracy (less than 1% error) in an approximate gauge, in which only two perturbed field equations need to be solved, allowing a larger number of grid points to be used. The approximate gauge is defined by equations (11)-(14) supplemented by the approximations

$$\frac{h_{tt}}{g_{tt} + 2\omega g_{t\phi}} = \frac{h_{rr}}{g_{rr}} = \frac{h_{\theta\theta}}{g_{\theta\theta}}, \quad (20)$$

and

$$h_{t\theta} = h_{r\phi} = 0. \quad (21)$$

Equation (20) enforces a similar relation between the diagonal components of h_{ab} , as in the Newtonian limit, while equation (21) essentially ignores the axial contribution to the metric perturbation (the axial contribution to the fluid velocity perturbation is retained). All results in the present paper will be obtained using the approximate gauge. Eight basis functions are used in equation (15), corresponding to $j = 0..3$ and $k = 0, 1$.

3. Improved Numerical Implementation

In SF, a highly accurate finite-difference scheme was used for the angular variable, that allowed the use of only a few angular spokes. This finite-difference scheme requires the solution to be a very smooth function and it gave accurate results for relativistic polytropes of index $N \geq 1.0$. Realistic EOSs have, however, a stiff interior and a sudden drop in density near the surface. Hence, the finite difference scheme used in SF would suffer from the Gibbs phenomenon at the surface of the star, if it were applied to realistic EOSs. This would result in an error of several percent in the determination of neutral modes for these equations of state.

Here, we use for the angular variable the same standard three-point finite difference scheme as used for the radial variable in SF. With a fine enough grid, the density distribution near the surface is resolved accurately (see section 4).

Another improvement is the use of Ridder’s method (see e.g. Press et. al. 1992) for locating the exact point along a sequence of rotating stars, where the determinant goes through zero. In SF, linear interpolation between two nearby stars was used.

4. Equations of State

The critical neutron star models for a set of EOSs were computed using the method described in the preceding section. Four realistic EOSs, A, C, L and WFF3, spanning a wide range of stiffness, were selected. Equations of state A, C and L are labeled as in Arnett & Bowers (1977). Equation of state A is one of the softest EOSs allowing a nonrotating $1.4M_{\odot}$ neutron star. Equation of state C has intermediate stiffness, while EOS L is one of the stiffest realistic EOSs. Equation of state WFF3 (UV14+TNI in Wiringa, Fiks, & Fabrocini 1988) is a modern EOS. At lower densities we match it to EOS FPS (Lorenz, Ravenhall, & Pethick 1993), which accurately describes the crust of a neutron star (see Nozawa et al. 1998 for

more details on the EOSs).

All realistic EOSs examined have an adiabatic index Γ , which is larger than 2.0 at the center and for most of the interior of the star. Thus, the equilibrium models are similar to stiff polytropic models with index $N = 1/(\Gamma - 1) < 1.0$. For such polytropic models, the Eulerian perturbation in the energy density diverges at the surface. This poses a potential threat to our numerical scheme since the integrand of equation (18) depends on $\delta\epsilon$ (cf. eq. (C24) of SF). Although the integral (18) is formally finite, the divergence of $\delta\epsilon$ at the star’s surface would make it difficult to accurately evaluate the integral. Skinner and Lindblom (1996) avoided this problem by using analytic expressions for the divergence of $\delta\epsilon$ in the case of Newtonian polytropes. In the realistic EOSs which we examined, this problem is not encountered because the EOSs soften near the star’s surface. In Figure 1, we plot the expression $(\epsilon + P)^2/P\Gamma$, which is proportional to $\delta\epsilon$, near the surface and the adiabatic index Γ , as a function of radial coordinate distance (in the equatorial plane) for representative equilibrium models constructed with EOSs C and L. As can be seen, the adiabatic index becomes less than $\Gamma = 2.0$ near the surface, so that $\delta\epsilon$ goes to zero, as occurs in soft polytropes of index $N > 1.0$. With enough grid-points in the radial direction, this change in $\delta\epsilon$ can be resolved accurately. Note that $(\epsilon + P)^2/P\Gamma$ has a maximum at *exactly* the points in the interior of the star, where the adiabatic index becomes $\Gamma = 2.0$. The vertical axis in Figure 1 is dimensionless (we set $c = G = 1$ and the length scale equal to $c/\sqrt{G\epsilon_0}$, where $\epsilon_0 = 10^{15}\text{g/cm}^3$).

The critical curves we obtain for the four realistic EOSs are also representative of the critical curves that one would obtain for stiff polytropes, if one correctly handled the divergence of $\delta\epsilon$ at the surface or matched a soft polytropic surface to a stiff polytropic interior. For example, models constructed with EOS C are roughly similar to polytropic models of index $N \sim 0.7$, while models constructed with EOS L are roughly similar to polytropic models of index $N \sim 0.5$.

5. Critical curves for realistic equations of state

Results for each equation of state are summarized in Tables 1 and 2 and Figures 2 to 5. The tables list equilibrium properties of the critical stars for a few selected examples. For each value of m , three stars were selected: a low mass star, a star with mass close to $1.4M_{\odot}$ and a star close to the maximum mass

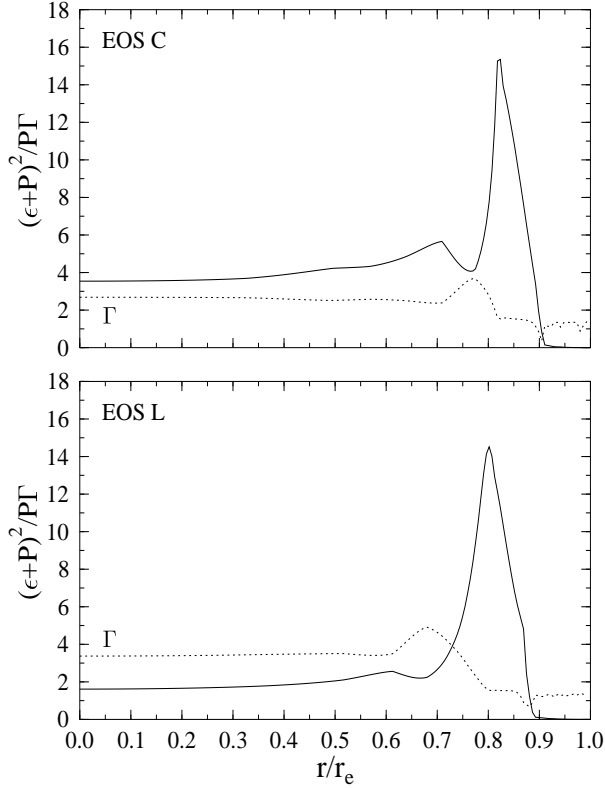


Fig. 1.— Behaviour of $(\epsilon + P)^2/P\Gamma$ (solid line) and Γ (dotted line) in the equatorial plane, as a function of coordinate radius (r_e is the coordinate radius at the equator). A $1.44M_\odot$ EOS C model (upper panel) and a $1.38M_\odot$ EOS L model (lower panel), belonging to the $l = m = 2$ neutral mode sequence are shown. The units of the vertical axis are explained in the text. Note that the divergence of $(\epsilon + P)^2/P\Gamma$ at the surface is avoided by a softening of the EOS (Γ becomes less than 2.0).

stable star along each neutral mode sequence. The following quantities are displayed in the tables:

ϵ_c central energy density

T/W ratio of rotational energy to gravitational potential energy

Ω_c critical angular velocity

Ω_c/Ω_K ratio of critical angular velocity Ω_c to the mass-shedding limit Ω_K at same central energy density

M gravitational mass

M_0 rest mass

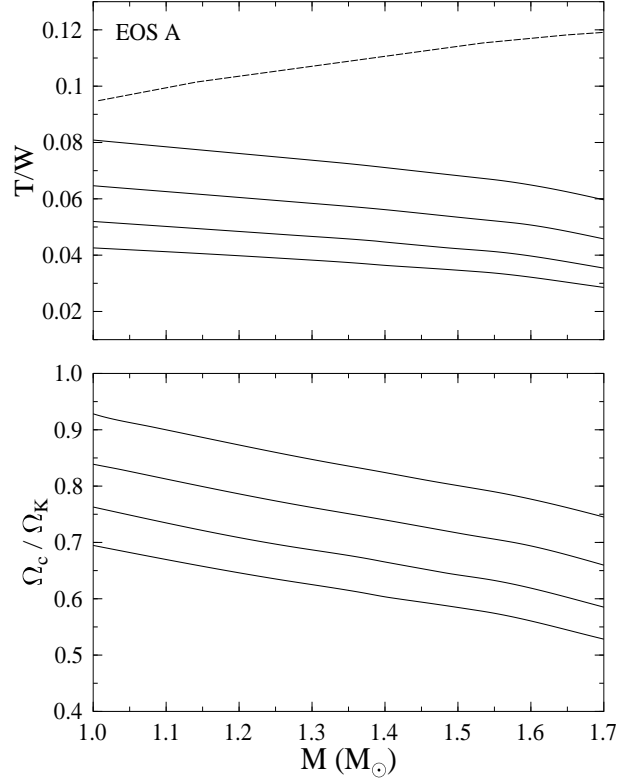


Fig. 2.— Neutral mode sequences for EOS A. Shown are the ratio of rotational to gravitational energy T/W (upper panel) and the ratio of the critical angular velocity Ω_c to the angular velocity at the mass-shedding limit for uniform rotation (lower panel) as a function of gravitational mass. The solid curves are the neutral mode sequences for $l = m = 2, 3, 4$ and 5 (from top to bottom), while the dashed curve in the upper panel corresponds to the mass-shedding limit for uniform rotation.

R equatorial circumferential radius

The $l = m = 2$ bar mode has the fastest growth time and will be the most efficient mode for the emission of gravitational radiation. For $1.4M_\odot$ stars, the bar mode is unstable for $\Omega/\Omega_K > 0.83$ for the softest EOS A and for $\Omega/\Omega_K > 0.93$ for EOS C. This corresponds to critical spin periods of 0.8 ms and 1.1 ms for EOSs A and C respectively. For maximum mass stars, the bar mode is unstable for $\Omega/\Omega_K > 0.69$ at $M = 2.9M_\odot$ for the stiffest EOS L and $\Omega/\Omega_K > 0.77$ at $M = 2.0M_\odot$ for EOS C.

In terms of T/W , the $l = m = 2$ mode becomes unstable at $T/W \sim 0.071 - 0.086$ for $1.4M_\odot$ stars and at $T/W \sim 0.06$ for the maximum mass along the neutral

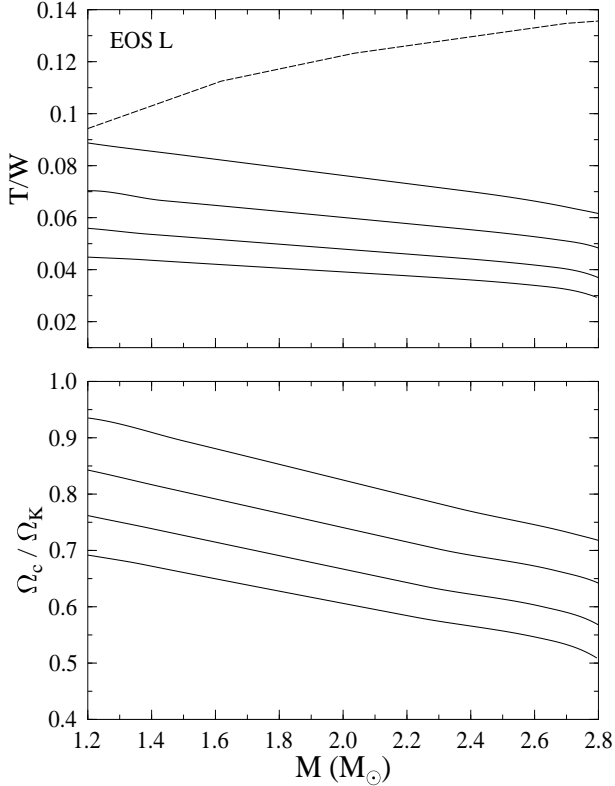


Fig. 3.— Same as Figure 2 but for EOS L.

mode sequence. The latter value is surprisingly insensitive to the equation of state. In fact, the $l = m = 2$ neutral mode sequence can be approximated by the following linear empirical formula,

$$(T/W)_2 = 0.115 - 0.048 \frac{M}{M_{\text{max}}^{\text{sph}}}, \quad (22)$$

where $M_{\text{max}}^{\text{sph}}$ is the maximum mass for a spherical star allowed by a given equation of state. The empirical formula has an accuracy of roughly 4%–6% for all values of M , except for stars near the axisymmetric stability limit, that is, near the maximum mass along the neutral mode sequence, where it is somewhat larger, (the T/W vs. M curves deviate somewhat from linearity, as can be seen in figs. 2 to 5). While in the Newtonian limit the bar mode becomes unstable at $T/W \sim 0.14$, in realistic $1.4M_{\odot}$ neutron stars the onset of the bar mode instability is at roughly 1/2 to 2/3 the Newtonian estimate of T/W .

The critical curves for the $l = m = 3, 4$ and 5 modes appear at successively lower rotation rates. All critical curves for all EOSs are nearly linear in gravitational mass and similar empirical formulae for these

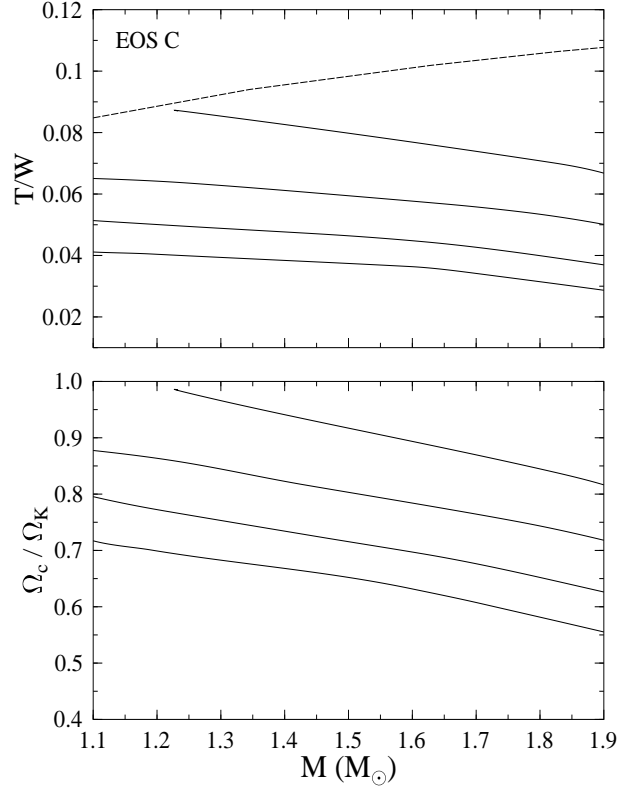


Fig. 4.— Same as Figure 2 but for EOS C.

modes can also be written, as in equation (22).

The obtained critical curves assume a perfect fluid. We expect that including the effects of viscosity will raise the critical angular velocities by a few percent in the 10^9K to 10^{10}K temperature window. The strengthening of the instability by relativistic effects will also widen the temperature window in which the instability will be active, as was already shown by post-Newtonian computations (Cutler & Lindblom 1992, Lindblom 1995).

By doubling the number of grid-points in both directions and from comparisons with the Newtonian limit and with the results in SF, we estimate the accuracy of our present results to be at the 1% level. Increasing the number of basis functions in equation (15) to more than eight, did not affect the critical curves by more than 1%.

6. Discussion

We find that for a wide range of realistic EOSs the polar $l = m = 2$ bar mode is unstable to the emission of gravitational waves in newly-born $1.4M_{\odot}$ neutron

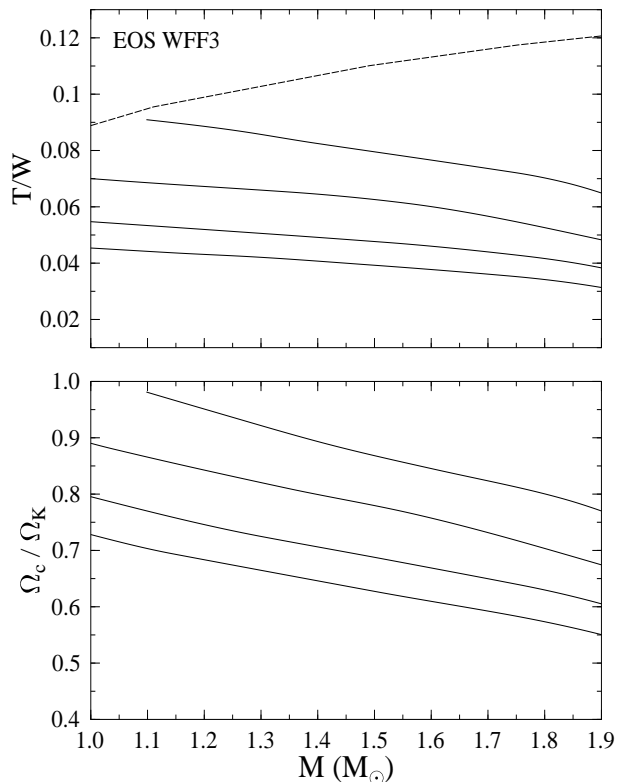


Fig. 5.— Same as Figure 2 but for EOS WFF3.

stars, rotating close to the Kepler limit, until their angular velocity falls below 83% – 93% of the Keplerian value. The recent observation of the fastest rotating young pulsar in the supernova remnant N157B (Marshall et al. 1998) suggests that a fraction of neutron stars born in supernovae are born with very large initial rotational energy. If some neutron stars are born in accretion-induced collapse of white dwarfs (Friedman 1983), they are also expected to have a large initial spin. Since it is initially very hot and differentially rotating, a proto-neutron star can even be born with an angular velocity exceeding the mass-shedding limit for uniformly rotating stars. As the star cools and passes through the temperature window of 10^9K to 10^{10}K , the nonaxisymmetric bar mode, driven by gravitational radiation, will grow and the star will lose angular momentum by the emission of gravitational waves. Within a short time, the star will have slowed down enough that the bar mode will become stable again. During this first phase the r -mode instability will also be operating. The r -mode instability will then continue to slow down the star, until the star reaches a period of roughly 6 – 9 ms, when the insta-

bility will be damped by viscosity.

The above picture assumes that the star cools through the standard modified URCA cooling scenario. If instead neutron stars cool very rapidly through e.g. the direct URCA process, then the instability in f -modes may not have enough time to grow significantly and the rotational evolution of the star will only be affected by the r -mode instability.

The CFS-instability in the bar f -mode appears to be a good source of detectable continuous gravitational waves. Lai & Shapiro (1995) have studied the development of the f -mode instability using Newtonian ellipsoidal models of rotating stars (Lai, Rasio, & Shapiro 1993, 1994). They consider the case where a neutron star is created in a core collapse with large initial angular momentum. After a brief dynamical phase, the proto-neutron star becomes axisymmetric but secularly unstable. The instability deforms the star into a nonaxisymmetric configuration via the $l = m = 2$ bar mode. As the star slows down, the frequency of the gravitational waves sweeps downward from a few hundred Hz to zero, passing through LIGO’s ideal sensitivity band. A rough estimate of the wave amplitude shows that, at $\sim 100\text{Hz}$, the gravitational waves from the CFS-instability could be detected out to the distance of 30 Mpc by LIGO or VIRGO and to 140Mpc by the advanced LIGO detector. This result is very promising, especially since for relativistic stars the instability will be stronger than in the Newtonian computations.

Another astrophysical situation in which the instability may have the opportunity to grow is after the merger of two neutron stars in a binary coalescence. Recently, Baumgarte & Shapiro (1998) studied the case in which the merged neutron star is unstable to collapse, but has more angular momentum than required to collapse to a Kerr black hole. They find that neutrino emission is inefficient for shedding the excess angular momentum of the neutron star and suggest that this can happen through the growth of the gravitational radiation driven bar f -mode. We expect the gravitational waves from the instability in these high mass ($M > 2.8M_\odot$) merged neutron stars to be especially strong and a detailed, fully relativistic study is needed.

The computation of quasi-normal finite-frequency modes of rapidly rotating relativistic stars is a more difficult problem than the neutral-mode calculation presented in this paper. The main difficulty is in applying the boundary conditions at infinity. Lindblom, Mendell and Ipser (1997) have recently pro-

posed an approximate near-zone boundary condition which appears to be a promising approach for solving for the complex eigen-frequencies. We plan to incorporate the near-zone boundary conditions into the SF method to allow the approximate computation of frequencies and growth times of the quasi-normal modes with reasonable accuracy.

It is a pleasure to thank John Friedman for helpful discussions and Nils Andersson for a critical reading of the manuscript. We also thank S. Yoshida and Y. Eriguchi for providing us with graphs of critical curves for two realistic equations of state, obtained in the Cowling approximation, before their publication. N.S. and S.M.M. acknowledge the generous hospitality of the Max-Planck-Institute for Gravitational Physics (Albert-Einstein-Institute) in Potsdam, Germany. This work was supported in part by NSF grant PHY 95-07740 and by NSERC of Canada.

REFERENCES

- Andersson, N. 1998, ApJ, in press, preprint available as gr-qc/9706075
- Andersson, N., Kokkotas, K., & Schutz, B. F. 1998, preprint, gr-qc/9805225
- Arnett, W. D., & Bowers, R. L. 1977, ApJ Sup., 33, 415
- Baumgarte, T. W., & Shapiro, S. L. 1998, ApJ, in press, preprint available as astro-ph/9801294
- Bonazzola, S., Friebe, J., & Gourgoulhon, E. 1998, A&A 331, 280
- Chandrasekhar, S. 1970, Phys. Rev. Lett., 24, 611
- Cutler, C. 1991, ApJ, 374, 248
- Cutler, C. & Lindblom, L. 1987, ApJ, 314, 234
- Cutler, C. & Lindblom, L. 1992, ApJ, 385, 630
- Cutler, C., Lindblom, L., & Splinter, R. J. 1990, ApJ, 363, 603
- Friedman, J. L. 1978, Commun. Math. Phys., 62, 247
- Friedman, J. L. 1983, Phys. Rev. Lett. 51, 11
- Friedman, J. L. & Ipser, J. 1992, Phil. Trans. R. Soc. Lond. A, 340, 391
- Friedman, J. L., & Morsink S. M. 1998, ApJ, in press, preprint available as gr-qc/9706073
- Friedman, J. L. & Schutz, B. F. 1978, ApJ, 222, 281
- Imamura, J. N., Friedman, J. L., & Durisen, R. H. 1985, ApJ, 294, 474
- Ipser, J. R., & Lindblom, L. 1990, ApJ, 355, 226
- Ipser, J. R., & Lindblom, L. 1991, ApJ, 373, 213
- Ipser, J. R., & Lindblom, L. 1992, ApJ, 389, 392
- Lai, D., Rasio, F. A., & Shapiro, S. L. 1993, ApJ Suppl., 88, 205
- Lai, D., Rasio, F. A., & Shapiro, S. L. 1994, ApJ, 373, 213
- Lai, D., & Shapiro, S. L. 1995, ApJ, 442, 259
- Lindblom, L. 1995, ApJ, 438, 265
- Lindblom, L., Owen, B. J., & Morsink, S. M. 1998, Phys. Rev. Lett., in press, preprint available as gr-qc/9803053
- Lorenz, C. P., Ravenhall, D. G., & Pethick, C. J. 1993, Phys. Rev. Lett., 70, 379
- Managan, R. A. 1985, ApJ, 294, 463
- Marshall, F. E., Gotthelf, E. V., Zhang, W., Middleton, J., & Wang, Q. D. 1998, ApJ, 499, L179
- Nozawa, T., Stergioulas, N., Gourgoulhon, E., & Eriguchi, Y. 1998, A&A, in press, preprint available as gr-qc/9804048
- Papaloizou, J. & Pringle, J. E. 1978, MNRAS, 182, 423
- Press, W. H., Teukolsky, S., Vetterling, W. T., & Flannery, B. P. 1992, Numerical Recipes in C, Second Edition, (Cambridge: Cambridge University Press)
- Regge, T., & Wheeler, J. A., 1957, Phys. Rev., 108, 1063
- Shapiro, S. L., & Zane, S. 1997, preprint, gr-qc/9711050
- Skinner, D., & Lindblom, L. 1996, ApJ, 461, 920
- Stergioulas, N. 1996, The Structure and Stability of Rotating Relativistic Stars, PhD Thesis, University of Wisconsin-Milwaukee, Milwaukee, USA

Stergioulas, N., 1998, Rotating Stars in Relativity, to appear in Living Reviews in Relativity, <http://www.livingreviews.org/>, preprint available as gr-qc/9805012

Stergioulas, N. & Friedman, J. L. 1998, ApJ, 492, 301

Wiringa, R.B., Fiks, V. & Fabrocini, A. 1988, Phys. Rev. C 38, 1010

Yoshida, S., & Eriguchi, Y. 1995, ApJ, 438, 830

Yoshida, S., & Eriguchi, Y. 1997, ApJ, 490, 779

Yoshida, S., & Eriguchi, Y. 1998, private communication

TABLE 1
NEUTRAL MODE SEQUENCES FOR EOS A AND EOS L

	ϵ_c ($\times 10^{15} \text{g/cm}^3$)	T/W	Ω_c ($\times 10^3 \text{s}^{-1}$)	Ω_c/Ω_K	M (M_\odot)	M_0 (M_\odot)	R (km)
EOS A							
$m = 2$	1.00	0.082	6.58	0.94	0.97	1.04	12.4
	1.50	0.071	7.46	0.83	1.40	1.55	11.2
	3.20	0.056	9.25	0.72	1.76	2.06	9.4
$m = 3$	1.00	0.066	6.02	0.86	0.94	1.00	11.7
	1.60	0.056	6.90	0.74	1.41	1.58	10.7
	3.20	0.044	8.28	0.65	1.73	2.03	9.3
$m = 4$	1.00	0.054	5.50	0.79	0.91	0.97	11.3
	1.62	0.045	6.28	0.67	1.40	1.57	10.5
	3.20	0.035	7.42	0.58	1.71	2.00	9.2
$m = 5$	1.00	0.044	5.04	0.72	0.89	0.95	11.0
	1.68	0.036	5.80	0.60	1.41	1.58	10.3
	3.20	0.029	6.76	0.53	1.70	1.99	9.1
EOS L							
$m = 2$	0.35	0.089	4.08	0.96	1.20	1.27	18.9
	0.38	0.086	4.20	0.91	1.38	1.48	18.3
	1.20	0.057	5.67	0.69	2.90	3.43	15.1
$m = 3$	0.35	0.070	3.70	0.87	1.14	1.21	17.5
	0.40	0.067	3.88	0.81	1.44	1.54	17.2
	1.20	0.045	5.10	0.62	2.85	3.38	14.9
$m = 4$	0.35	0.056	3.38	0.79	1.10	1.16	16.8
	0.40	0.054	3.53	0.74	1.39	1.50	16.6
	1.20	0.036	4.58	0.56	2.82	3.34	14.7
$m = 5$	0.35	0.046	3.09	0.73	1.08	1.13	16.3
	0.40	0.044	3.23	0.68	1.36	1.46	16.3
	1.20	0.029	4.16	0.51	2.79	3.31	14.6

TABLE 2
NEUTRAL MODE SEQUENCES FOR EOS C AND EOS WFF3

	ϵ_c ($\times 10^{15} \text{g/cm}^3$)	T/W	Ω_c ($\times 10^3 \text{s}^{-1}$)	Ω_c/Ω_K	M (M_\odot)	M_0 (M_\odot)	R (km)
EOS C							
$m = 2$	0.74	0.087	5.48	0.99	1.23	1.32	16.4
	0.90	0.082	5.92	0.93	1.44	1.56	14.9
	2.50	0.059	8.13	0.77	2.00	2.30	11.2
$m = 3$	0.70	0.066	4.75	0.89	1.11	1.18	14.9
	0.95	0.061	5.38	0.82	1.43	1.56	13.8
	2.50	0.046	7.30	0.69	1.96	2.26	11.0
$m = 4$	0.70	0.052	4.29	0.80	1.07	1.14	14.2
	1.00	0.047	4.94	0.73	1.45	1.58	13.2
	2.50	0.036	6.48	0.62	1.94	2.23	10.8
$m = 5$	0.70	0.042	3.91	0.73	1.05	1.11	13.8
	1.00	0.038	4.46	0.65	1.42	1.55	12.9
	2.50	0.028	5.79	0.55	1.92	2.20	10.7
EOS WFF3							
$m = 2$	0.80	0.091	6.09	0.98	1.10	1.17	14.6
	1.00	0.083	6.56	0.89	1.40	1.53	13.2
	2.50	0.059	8.33	0.74	1.98	2.31	10.7
$m = 3$	0.70	0.072	5.17	0.94	0.86	0.90	13.9
	1.05	0.063	5.99	0.79	1.40	1.55	12.5
	2.50	0.046	7.44	0.66	1.95	2.27	10.5
$m = 4$	0.70	0.057	4.68	0.85	0.82	0.87	13.0
	1.10	0.051	5.55	0.71	1.43	1.58	12.1
	2.50	0.037	6.73	0.60	1.92	2.24	10.4
$m = 5$	0.70	0.047	4.31	0.79	0.80	0.85	12.6
	1.10	0.042	5.09	0.65	1.40	1.55	11.8
	2.50	0.031	6.18	0.55	1.91	2.23	10.3